BCSIR

Available online at www.banglajol.info/index.php/BJSIR

Bangladesh J. Sci. Ind. Res. **59(3)**, 129-138, 2024

BANGLADESH JOURNAL OF SCIENTIFIC AND INDUSTRIAL RESEARCH

ISSN. 0304-9809

Structural, mechanical and electronic properties of Zr_2SeB MAX phase through DFT approach at ambient and elevated pressures

I. Ahmed, M. A. Kashem*, M. S. Islam and K. N. Babi

Physical Instrumentation Division, BCSIR Laboratories, Dhaka, Bangladesh Council of Scientific and Industrial Research (BCSIR), Dhaka-1205, Bangladesh

ARTICLE INFO

Received: 30 August 2023

Revised: 26 May 2024

Accepted: 30 June 2024

eISSN 2224-7157/

DOI: https://doi.org/10.3329/bjsir.v59i3.66920

Abstract

The DFT approach is used in the pressure range of 0 - 50 GPa to examine the physical characteristics of the synthesized MAX phases Zr_2SeB for the first time. The calculated lattice parameters agree with previous findings at ambient pressure. The density of states and band structure exhibit that within the studied pressure range, Zr_2SeB is metallic. Under various pressures, partial DOS is also taken into consideration. The investigated compound maintains their mechanical stability up to 50 GPa. Zr_2SeB is elastically anisotropic up to 50 GPa, and brittle up to 20 GPa pressure. The brittleness of the material decreases with increasing pressure. At 30, 40 and 50 GPa, however, Zr_2SeB exhibit a ductile behavior. The MAX phase research community is anticipated to be inspired by this discovery to further investigate the properties of this material under various pressures.

Keywords: MAX phase; DFT study; Mechanical properties; Band structure; Density of states; Pressure effects

Introduction

A family of layered ternary carbides and nitrides with the general formula $M_{n+1}AX_n$, where n = 1-3, M is an early transition metal, A is a p-block element, and X is B or C or N are called MAX phases. These intriguing nanolaminates have a unique mix of physical, chemical, mechanical and electrical, characteristics, making them thermodynamically stable materials with a wide range of possible applications. These are thermodynamically stable nanolaminates and are interesting materials with great application potential due to their remarkable combination of chemical, physical, electrical and mechanical properties (Barsoum, 2001). Like metals, they are extraordinarily damage resistant, electrically and thermally conductive, plastic at high temperatures, and most easily machinable. (Barsoum and El-Raghy, 1996; El-Raghy *et al.* 1999; Sun *et al.* 2006). Like ceramics, they are lightweight, elastically rigid, fatigue, creep, maintain their strengths to high temperatures and oxidation and corrosion resistant (Barsoum, 2009; Sundberg *el al.* 2004; Jovic *el al.* 2006). MAX phases are intriguing prospects for applications in the nuclear sector, superconducting materials, spintronics, wear and corrosion-resistant coatings, high-temperature technologies, Li-ion batteries, sliding, contacts for 2D electronic circuits and electrical contacts (Barsoum, 2013; Surucu, 2018; Ali *et al.* 2018). The hybrid features of MAX phases are caused by the presence of strong covalent M-X bonds and relatively weak metallic M-A links inside their structure. These challenging traits are a perpetual source of inspiration for scientists, and as a result, more than 150 MAX stages have been found (Sokol *et al.* 2019).

*Corresponding author's e-mail: kashem@bcsir.gov.bd

Additionally, scientists are attempting to alter composition and structure to attain an excellent mix of properties, including various alloys or solid solutions, (Lapauw *et al.* 2018; Tunca *et al.* 2019; Griseri *et al.* 2020; Ali and Naqib, 2020) M_2A_2X, (He *et al.* 2018; Chen *et al.* 2019) and M_3A_2X, (Chen *et al.* 2019) rare-earth i-MAX phases, (Tao *et al.* 2019; Ali *et al.* 2021), 212 MAX phases, (Miao *et al.* 2020) 314 MAX phases,(Ali *et al.* 2021) MAX phase borides (Rackl *et al.* 2019; Rackl and Johrendt, 2020; Ali *et al.* 2021) and MXenes, the derivatives of the two-dimensional (2D) MAX phase (Naguib *et al.* 2011).

Ti_2SC and Zr_2SC were included in a thorough analysis of the elastic characteristics of the 211 MAX phases that Cover *et al.* performed (Cover *et al*. 2009). After synthesizing M_2SB (M = Zr, Hf, and Nb) borides, Rackl *et al*. (2020) exposed them to a thorough examination on the basis of M_2SX's (X = C and B) physical characteristics. In each instance, the mechanical properties of the S-containing MAX phases outperform those of the comparable Al-containing MAX phases. Chen *et al.* (2021) recently developed a novel chalcogen (Se) containing MAX phase (Zr_2SeC). The electrical resistivity, electronic density of the different states, thermal conductivity, and the charge density of Zr_2SeC were investigated, and Qiqiang Zhang *et al.* (2022) synthesized Zr_2SeB. In numerous fields where several different MAX phases have already been used, these inadequate Zr_2SeB results are not sufficient for practical use. Therefore, a detailed study of Zr_2SeB must thus be thoroughly studied in order to reap the benefits and be used in as many industries as feasible. As a result, this work presents the structural, mechanical and electronic characteristics of Zr_2SeB at zero and high pressure. The remaining text is arranged as follows: The entire computational methodology is presented in Section 2, the findings and analysis are presented in Section 3, and the main conclusions are presented in Section 4.

Materials and methods

First-principles calculations were performed within the context of density functional theory (Kohn and Sham, 1965) by utilizing the plane-wave pseudopotential method applied in the CASTEP code (Clark *et al.* 2005). Ultra-soft pseudopotentials created by Vanderbilt were used to model the interaction between electrons and ion cores (Vanderbilt, 1990). The generalized gradient approximation (GGA) is used to address the electronic exchange and correlation energies, according to Perdew-Burke-Ernzerhof (PBE) (Perdew *et al.* 1996). The Broyden-Fletcher-Goldfarb-Shanno (BFGS) minimization technique (Fischer and Almlof, 1992) is used to . determine a crystal's ground state. By independently altering the lattice parameters and internal locations of atoms leaving core correction or spin effect, the crystal structures are totally optimized. A Γ-centered k-point mesh of 23×23×5 grid is employed to integrate over the first Brillouin zone of the reciprocal space of the hexagonal unit cell of MAX phases (Monkhorst and Pack, 1996) in the Monkhorst–Pack (MP) scheme. A planewave cutoff energy of 700 eV was found to be suitable for expanding the eigenfunctions of valence and nearly valence electrons of the atoms of the systems. In order to achieve geometry optimization, the tolerance for convergence is being set to an energy change of less than 10^{-5} eV/atom, a force change below 0.03 eV, a stress change below 0.05 GPa, and a change of atomic displacement below 10^{-3} Å. The CASTEP code's implementation of the stress-strain method (Nielsen and Martin 1983) is performed to determine the elastic constants, C_{ij}. DFT is a suitable approach for characterizing the electrical structure of crystalline materials (Hadi, 2016; Hadi *et al.* 2009).

Results and discussion

Structural properties

Experimental and theoretical studies have crystallized the Zr_2SeB in Hexagonal structure with lattice parameter '*a*' and '*c*' , space group $P6_3/mmc$ (194) (Barsoum, 2013). The unit cell has eight atoms since it is comprised of two formula units. The atomic positions of Zr_2SeB are Zr: (1/3, 2/3, 0.6029), Se: (1/3, 2/3, 1/4), and B: (0, 0, 0) (Zhang *el at.* 2022). Fig. 1(a) depicts the unit cell of the crystal structures of Zr_2SeB where the atoms are specified separately by different colors and Fig. 1(b) represents its two dimensional view in xy plane. From this figure it is observed that, the Se atom is sandwiched between two Zr_2SeB octahedra. Table I provides the optimal lattice parameters for comparison along with the relevant experimental and theoretical data. Table I shows how pressure affects the lattice parameters of Zr_2SeB. With rising pressure, it is seen that the lattice parameters are decreasing; accordingly, a similar trend is seen for volume. The pressure dependence of the lattice parameters '*a*' and '*c*' for Zr_2SeB is plotted in Fig. 2(a) with increments of 10 GPa from 0 to 50 GPa. It is also revealed from this figures that the lattice parameter '*a*' and '*c*' decreases successively with increasing pressure. Further we also observed that the lattice parameters '*a*' and '*c*', respectively, varied by 29% and 74% with increasing pressure. The compression along the '*c*' direction is therefore lower than that along the '*a*' direction, as shown by Table I and Fig. 2(a), where the lattice parameter '*c*' falls with pressure more quickly than the lattice parameter '*a*'. Figures 2(b), 2(c), and 2(d) show, respectively, the pressure dependence of the normalized lattice parameters (a/a_0 and c/c_0, where a_0 and c_0 are the equilibrium lattice

parameters.), volume, and the unit cell's normalized volume. From these figures it is seen that both a/a_0 and c/c_0 tend to decrease with pressure due to the fact that pressure compresses the volume. Furthermore, based on this research, it is predicted that when pressure rises, the bonds in Zr_2SeB would get strong and the bond lengths will shorten.

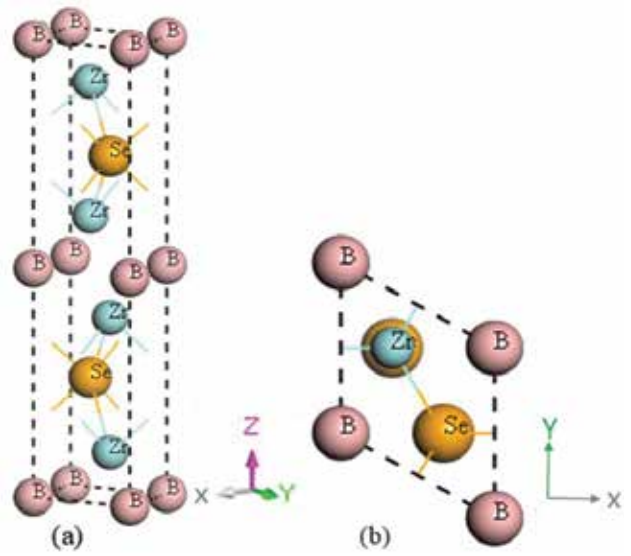

Fig. 1. (a) Crystal structure of Zr_2SeB, (b) 2D view in the xy-plane

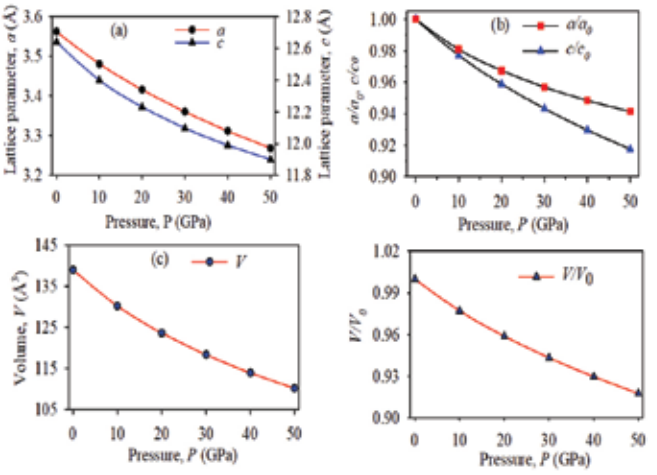

Fig. 2. (a) Lattice parameters, (b) Normalized lattice parameters, (c) Volume and (d) Normalized volume of Zr_2SeB under pressure

including mechanical stability, anisotropic bonding strength, ductility, rigidity, and displacement. Using the strain-stress method, elastic constants (C_{ij}) are computed. Elastic constants can be used to evaluate a solid's mechanical stability. The elastic constants provide significant information, such as the interpretation of solid rigidity is known by C_{11} and C_{33}. Due to its hexagonal structure, Zr_2SeB possesses five distinct elastic constants. This group consists of C_{11}, C_{13}, C_{33}, C_{12}, and C_{44}. The following formula can be used to estimate the value of C_{66}, a second elastic constant that depends on C_{11} and C_{12}:

$$C_{66} = \frac{C_{11} - C_{12}}{2}$$

Table I. Estimated and available theoretical and experimental values of lattice constants (a and c, in Å), their ratio *c/a* and volume (V, in $Å_3$) for Zr_2SeB under various pressure (*P*, in GPa)

P	*a*	*c*	*c/a*	*V*	Remark
0	3.5624	12.6416	3.5486	138.9377	This study
	3.6440	12.6323	---	---	(Zhang *et al.* 2022)[exp]
	3.5624	12.6417	---	---	(Zhang *et al.* 2022)[theo]
10	3.4813	12.4006	3.5621	130.1565	This study
20	3.4159	12.2312	3.5807	123.6010	This study
30	3.3605	12.0974	3.5999	118.3159	This study
40	3.3119	11.9901	3.6203	113.8929	This study
50	3.2687	11.9005	3.6407	110.1212	This study

Mechanical stability and behaviors

A material's utility range can be measured using its mechanical relationships, which can also confirm the degree of service that is anticipated. The mechanical relationships can be used to identify the most prevalent solid characteristics,

Table II displays the computed values for the elastic constants of Zr_2SeB. Our calculated elastic constants meet the following stability requirements: (Qureshi *et al.* 2021; Sin'ko and Smirnov, 2002; Sin'ko and Smirnov, 2005; Anderson, 1963).

$C_{11} > C_{12}$, $C_{11} > 0$, $C_{33}(C_{11} + C_{12}) - 2(C_{13})^2 > 0$, and $C_{44} > 0$, and hence, Zr_2SeB is mechanically stable. Table II shows that for both compounds, $C_{11} < C_{33}$, showing that the compounds are required at a higher level of pressure to bend along the c-axis than the a-axis. As a function of hydrostatic pressure, Figure 3(a) displays the calculated elastic constants. The elastic constants grow monotonically with increasing pressure except C_{11}, C_{12}, C_{66} at pressures 30 and 40 GPa. In spite of the fact that Zr_2SeB maintains its mechanical stability at these pressures, C_{11}, C_{12}, and C_{66} demonstrate aberrant behavior.

A solid's Young's modulus (E) determines its stiffness, whereas its shear modulus (G) and bulk modulus (B) dictate its resistance to plastic deformation and incompressibility, respectively. The elastic constants C_{ij} can be used to compute the bulk modulus B and shear modulus G. For hexagonal crystals, these two moduli (noted B_V and G_V) may be computed using the Voigt approximation (Voigt, 1928) as:

The bulk and shear moduli (noted B_R and G_R) in the Reuss

$$B_V = \frac{1}{9}[2(C_{11} + C_{12}) + 4C_{13} + C_{33}]$$

$$G_V = \frac{1}{30}(C_{11} + C_{12} + 2C_{33} - 4C_{13} + 12C_{44} + 12C_{66})$$

approximation (Reuss and Angew, 1929) are defined as follows:

$$B_R = \frac{(C_{11} + C_{12})C_{33} - 2C_{13}^2}{C_{11} + C_{12} + 2C_{33} - 4C_{13}}$$

$$G_R = \frac{5C_{44}C_{66}[(C_{11} + C_{12})C_{33} - 2C_{13}^2}{2[3B_VC_{44}C_{66} + \{(C_{11} + C_{12})C_{33} - 2C_{13}^2\}(C_{44} + C_{66})]}$$

The arithmetic mean of the B and G effective values for anisotropic polycrystalline crystals as determined by the Voight and Reuss approximations is what is known as the Hill approximation (Hill, 1952):

$$B = \frac{1}{2}(B_R + B_V) \quad \text{and} \quad G = \frac{1}{2}(G_R + G_V)$$

Using the following formulae, Young's modulus E and Poisson's ratio v may be calculated from B and G (Karkour *et al.* 2022)

$$E = \frac{9BG}{3B + G} \quad \text{and} \quad v = \frac{3B - 2G}{2(3B + G)}$$

Fig. 3(b) and Table II can be used to show how pressure affects elastic modulus. As pressure increases, the bulk modulus, B, rises practically linearly. Apart from at 30 and 40 GPa pressure, the Young's modulus E and the Shear modulus G likewise rise with pressure. The stiffness of materials is often higher when the Young's modulus E is higher. Therefore, from the values of E as shown in Table III and figure 3(b), it can be said that Zr_2SeB is a stiff material and its stiffness increases with increasing pressure. The resistance to thermal shock is related to Young's modulus. High thermal shock resistance is marked by a low Young's modulus value. High thermal shock resistance is a requirement for the ideal thermal barrier coating (TBC) material. Therefore, from the values of E as shown in Table III, it can be said that Zr_2SeB is likely to be TBC materials.

Using Pugh's and Poisson's ratio, it was determined if the aforementioned composite was ductile or brittle at the investigated pressure range. Pugh's and Poisson's ratios of Zr_2SeB is shown at various pressures in Fig. 3(b). When G/B exceeds 0.57, a material is considered brittle by Pugh's ratio (Pugh 1954); otherwise, it is ductile. Again, it is generally known that a solid is brittle if the Poisson's ratio is less than 0.26, (Roknuzzaman *et al*. 2017) and ductile if it is higher. With the exception of 30, 40, and 50 GPa, at ambient pressure, both compounds are brittle and remain such for up to 20 GPa, as shown in Table III and Fig. 3(c), in accordance with the aforementioned threshold values. Zr_2SeB exhibit ductility at pressure 30, 40 and 50 GPa. The machinability index (*MI*), B/C_{44}, which governs the form flexibility of any material, is a crucial feature for the use of MAX phase. Table III contains a list of the *MI* of Zr_2SeB, and Fig. 3(c) shows it. These findings indicate that the *MI* of Zre_2SeB increases as pressure increases. It is well known that metallic compounds have a higher *MI* than ceramic ones. As Zr_2SeB is metallic and the *MI* value is increasing with increasing pressure thus it can be said that the metallicity is increasing with increasing pressure.

Table II. Estimated elastic constants, C_{ij} (GPa), of Zr_2SeB at different pressures, (P, in GPa)

P	C_{11}	C_{12}	C_{13}	C_{33}	C_{44}	C_{66}	Remark
0	242	72	78	263	113	85	This study
	228	87	77	266	109	71	(Zhang *et al.* 2022)
10	290	104	117	320	145	93	This study
20	340	126	153	377	175	107	This study
30	328	200	188	427	201	64	This study
40	349	244	223	472	226	52.5	This study
50	425	234	258	516	249	95.5	This study

Table III. Calculated elastic moduli values, all in GPa, Poisson's ratio, Pugh's ratio, machinability index of Zr_2SeB in the pressure range 0–50 GPa

P	B	G	E	υ	G/B	B/C_{44}	Remark
0	134	96	232	0.211	0.72	1.18	This study
	133	88	216	0.229	---	---	(Zhang *et al.* 2022)
10	175	111	276	0.237	0.63	1.21	This study
20	213	129	322	0.248	0.61	1.22	This study
30	247	112	293	0.302	0.45	1.23	This study
40	281	110	293	0.326	0.39	1.24	This study
50	316	145	378	0.301	0.45	1.27	This study

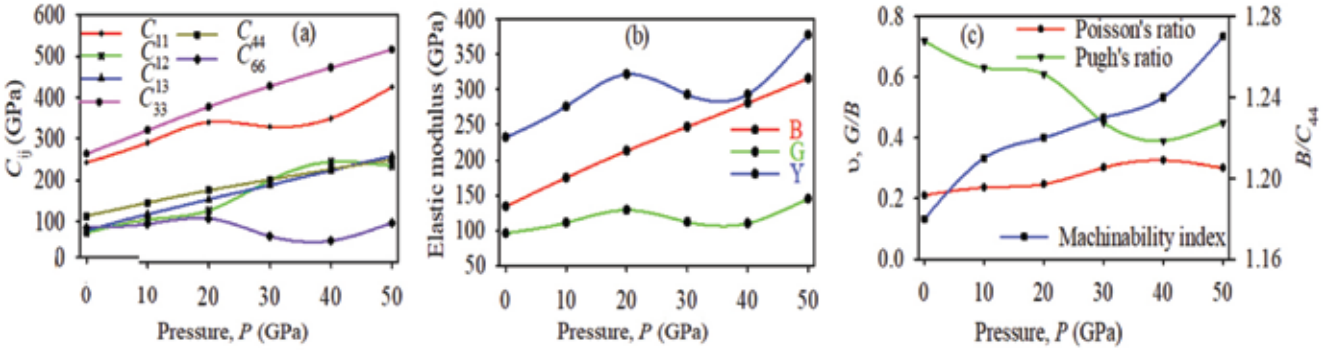

Fig. 3. (a) Elastic constants (C_{ij}), (b) Elastic moduli (*B, G,* and *Y*) and (c) Poisson's, Pugh's ratio and machinability index for Zr_2SeB at different pressures

The production of plastic deformation or the propagation of cracks is influenced by elastic anisotropy. The following formulae can be used to calculate the shear anisotropy factors (Ranganathan and Ostoja-Starzewski, 2008):

$$A_1 = \frac{C_{11} + C_{12} + 2C_{33} - 4C_{13}}{6C_{44}}$$

$$A_2 = \frac{2C_{44}}{C_{11} - C_{12}}$$

$$A_3 = \frac{C_{11} + C_{12} + 2C_{33} - 4C_{13}}{3(C_{11} - C_{12})}$$

where A_1 refers to the shear anisotropy in the {100} shear planes between the <011> and <010> directions, A_2 to the {010} shear planes between the <101> and <001> directions and A_3 to the share planes {001} between <110> and <010> directions. The relation between elastic anisotropy factor and the linear compressibility coefficient for a hexagonal crystal is given below (Hadi, 2016):

$$\frac{K_c}{K_a} = \frac{C_{11} + C_{12} - 2C_{13}}{(C_{33} - C_{13})}$$

Ranganathan and Osraja calculated the universal anisotropy index as follows (Ranganathan and Ostoja-Starzewski, 2008; Ledbetter, 1977)

$$A^U = 5\frac{G_v}{G_R} + \frac{B_v}{B_R} - 6$$

Table IV provides an illustration of the elastic anisotropy for Zr_2SeB under pressure and Shear anisotropy is shown in Fig. 4. The anisotropic elastic behavior of the Zr_2SeB phase show anisotropic nature upto 50 GPa pressure as A_i and $K_c/K_a = 1$ for isotropic situations. Additionally, for an isotropic condition, the value of A^U is equal to 0. Varying degrees of anisotropy are suggested by positive or negative values of A^U. Figure 4 demonstrates the anisotropy of both compounds up to a pressure of 50 GPa.

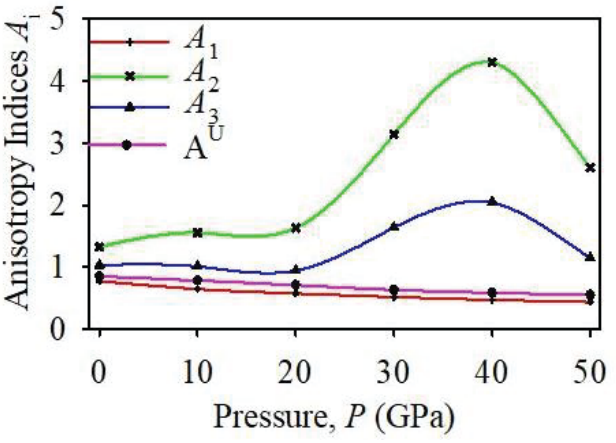

Fig. 4. Zr_2SeB's shear anisotropy factors in the 0–50 GPa pressure range

Electronic properties

Electronic band Structure

The energy of the crystal orbitals in a crystalline substance are represented in two dimensions by the band structure. In essence, it depicts the range of electronic energies that are allowed in a solid material. A solid's insulating, semi-metallic, or metallic nature can be explored using the band structure graph. By determining the properties and energy of the prominent bands close to the Fermi level, various aspects of a material can be investigated. From a band structure curve, one can extract significant details about a material, such as its electrical conductivity, optical properties etc. The Fermi surfaces form can be better understood by calculating the electronic band structure. A band structure has a number of bands that equals the number of atomic orbitals in a unit cell. The energy bands of Zr_2SeB in the range of -4 eV to 4 eV are computed and shown in Fig. 5(a) along the high symmetry directions

Table IV. Elastic anisotropy factors for Zr_2SeB in the pressure range 0–50 GPa

P	A_1	A_2	A_3	A^U	K_c/K_a	Remark
10	0.78	1.33	1.04	0.10	0.85	This study
20	0.65	1.56	1.01	0.25	0.79	This study
30	0.58	1.64	0.95	0.34	0.71	This study
40	0.52	3.14	1.64	1.47	0.64	This study
50	0.48	4.30	2.05	2.52	0.59	This study

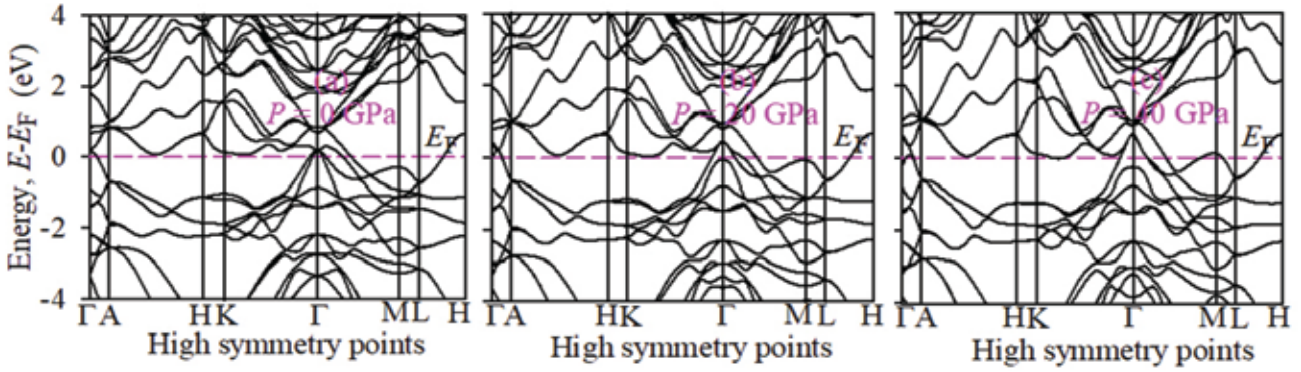

Fig. 5. Calculated band structures of Zr_2SeB along the high symmetry directions of the Brillouin zone at (a) $P = 0$ GPa (b) $P = 20$ GPa (c) $P = 40$ GPa, respectively. The Fermi energy is set to 0 eV, and the horizontal line represents it

(Γ-A-H-K-Γ-M-L-H) of the Brillouin zone at zero pressure. The line horizontally across the conduction and valance bands at zero energy is known as the Fermi level E_F. This graph demonstrates probable valance and conduction band overlap, which is a sign of metallic behavior. The variation of the band structure with pressure in the range from 0 to 40 GPa with steps of 20 GPa have been

Table V. Calculated total and partial density of states (states/eV) at the fermi level of Zr_2SeB at different pressures (P, in GPa)

Phase	P	Partial density of states, PDOSs at E_F							Calculated total DOS at E_F	Total DOS at E_F (from graph)	Ref.
		Zr			Se		B				
		5s	4p	4d	4s	4p	2s	2p			
Zr_2SeB	0	0.02	0.15	2.71	0.08	0.19	0.00	0.37	3.52	3.53	This
	20	0.02	0.19	2.66	0.10	0.28	0.01	0.55	3.81	3.80	This
	40	0.03	0.24	2.64	0.08	0.33	0.01	0.64	3.97	3.96	This

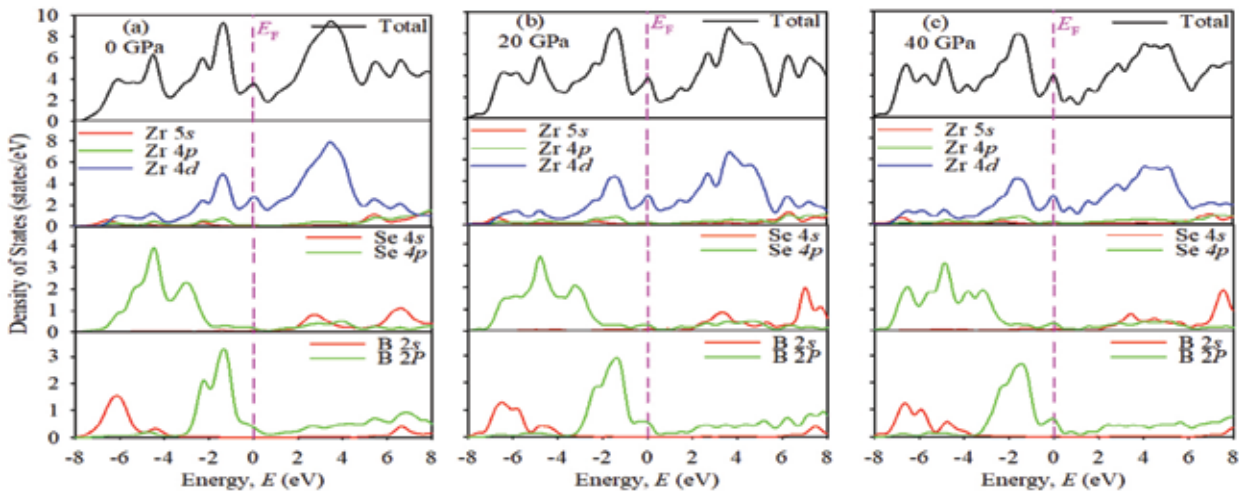

Fig. 6. Total and partial density of states of Zr_2SeB at (a) $P = 0$ GPa, (b) $P = 20$ GPa and (c) $P = 40$ GPa, respectively

investigated in this present study as shown in Figs. 5 (a), (b) and (c), respectively. These graphs reveal that the metallic behavior of Zr_2SeB remains constant up to a pressure of 40 GPa. The bands are pushed away from the Fermi level along the Γ, H and K directions and closer to it along the M, L directions with increasing pressure.

Density of States

The quantity of electron states in respect to both volume and energy is known as the density of states. The density of states has an effect on several bulk properties of conductive materials, including specific heat, paramagnetic susceptibility, and different transport phenomena. For Zr_2SeB at zero pressure, the computed total and partial density of states is shown in Fig. 6(a). The vertical line in this image depicts the Fermi level. Table V demonstrates that the density of states at the Fermi level is 3.52 at ambient pressure, which predominately contains contributions from the *Zr*-4d states, which have a contribution of 2.71, and the *B*-2p states, which have a contribution of 0.37, respectively. Further, the pressure effects on the electronic structure of Zr_2SeB is studied. The calculated total and partial density of states for Zr_2SeB at 20 and 40 pressures are tabulated into Table V and illustrated into Figs. 6(b) and 6(c), respectively. These figures show that with increasing pressure, the density of states for Zr_2SeB at the Fermi level rises. This implies that for Zr_2SeB, conductivity rises as pressure rises.

Conclusion

In conclusion, the DFT approach was used to analyze the structural, elastic, and electrical characteristics of Zr_2SeB while taking the pressure impact into consideration. The accuracy of the calculations utilized in this study is shown by the optimized lattice parameters' fair agreement with the data from the available experiments. According to the current study, the compression along the *c* direction is somewhat larger than along the *a* direction because the lattice parameter *c* lowers marginally more quickly than the lattice parameter *a*. Zr_2SeB is metallic at all examined pressures, as demonstrated by band structure and TDOS studies. The elastic constants in the investigated pressure range provide as evidence for the mechanical stability of Zr_2SeB. Additionally, the impact of pressure on the parameters relating to elastic moduli, elastic constants, and anisotropy is seen. It is demonstrated that pressure causes the values of the mechanical behavior-related parameters to rise. The compounds' brittleness, which tends to decrease with rising pressure, is revealed. The exploration of the MAX phase materials under high pressure is expected to be accelerated by the research's findings.

Acknowledgement

The High-Performance Computing (HPC) facility at the Condensed Matter Physics Lab, Department of Physics, University of Rajshahi, Rajshahi-6205, provided the computational capacity for the authors to determine the physical parameters of the Zr_2SeB MAX phase.

References

Ali MA, Hossain MM, Hossain MA, Nasir MT, Uddin MM, Hasan MZ, Islam AKMA and Naqib SH (2018), Recently synthesized $(Zr_{1-x}Ti_x)_2AlC$ $(0 \leq x \leq 1)$ solid solutions: Theoretical study of the effects of M mixing on physical properties, *J. Alloys Compd.* **743:** 146-154. DOI: 10.1016/j.jallcom.2018.01.396

Ali MA and Naqib SH (2020), Recently synthesized $(Ti_{1-x}Mo_x)_2AlC$ $(0 \leq x \leq 0.20)$ solid solutions: deciphering the structural, electronic, mechanical and thermodynamic properties *via ab initio* simulations, *RSC Adv.*, **10**: 31535-31546. DOI: 10.1039/d0ra06435a

Ali MA, Hossain MM, Islam AKMA and Naqib SH (2021), Ternary boride Hf_3PB_4: Insights into the physical properties of the hardest possible boride MAX phase, *J. Alloys Compd.* **857:** 158264. DOI: 10.1016/j.jallcom.2020.158264

Ali MA, Hossain MM, Uddin MM, Islam AKMA, Jana D and Naqib SH (2021), DFT insights into new B-containing 212 MAX phases: Hf_2AB_2 (A = In, Sn), *J. Alloys Compd.* **860**: 158408. DOI: 10.1016/j.jallcom.2020.158408

Ali MA, Hossain MM, Uddin MM, Hossain MA, Islam AKMA and Naqib SH (2021), Physical properties of new MAX phase borides M_2SB (M = Zr, Hf and Nb) in comparison with conventional MAX phase carbides M_2SC (M = Zr, Hf and Nb): Comprehensive insights, *J. Mater. Res. Technol.* **11**: 1000-1018. DOI: 10.1016/j.jmrt.2021.01.068

Anderson OL (1963), A simplified method for calculating the debye temperature from elastic constants, *J. Phys. Chem. Solids* **24:** 909 - 917. DOI: 10.1016/ 0022-3697(63)90067-2

Barsoum MW (2001), The $M_{N+1}AX_N$ phases: A new class of solids: Thermodynamically stable nanolaminates, *Prog. Solid State Chem*: **28**: 201-281. DOI: 10.1016/ S0079-6786(00)00006-6

Barsoum MW and El-Raghy T (1996), Synthesis and Characterization of a Remarkable Ceramic: Ti_3SiC_2, *J. Am. Ceram. Soc*. **79**: 1953-1956. DOI: 10.1111/j.1151-2916.1996.tb08018.x

Barsoum MW (2013), *MAX phases: Properties of machinable ternary carbides and nitrides, Wiley-VCH Verlag GmbH & Co. KGaA, Weinheim, Germany.* DOI: 10.1002/9783527654581

Barsoum MW (2009), Physical properties of the MAX phases, Encyclopedia of Materials: Science and Technology, *Elsevier, Amsterdam.* DOI: 10.1016/B0-08-043152-6/02058-1

Barsoum MW (2013), MAX phases: properties of machinable ternary carbides and nitrides, ISBN: 978-3-527-65460-4. DOI: 10.1002/9783527654581

Clark SJ, Segall MD, Pickard CJ, Hasnip PJ, Probert MIJ, Refson K and Payne MC (2005), First principles methods using CASTEP, *Zeitschrift fuer Kristallographie*, **220**: 567-570. DOI: 10.1524/zkri.220.5.567.65075

Cover MF, Warschkow O, Bilek MMM and McKenzie DR (2009), A comprehensive survey of M_2AX phase elastic properties, *J. Phys.: Condens. Matter* **21**(30): 305403. DOI: 10.1088/0953-8984/21/30/305403

Chen K, Bai X, Mu X, Yan P, Qiu N, Li Y, Zhou J, Song Y, Zhang Y, Du D, Chai Z and Huang Q (2021), *MAX Phase Zr_2SeC and Its Thermal Conduction Behavior, J. of the Euro. Cera Soc*. **41**(8): 4447-4451. DOI: 10.1016/j.jeurceramsoc.2021.03.013

Chen H, Yang D, Zhang Q, Jin S, Guo L, Deng J, Li X and Chen X (2019), A Series of MAX Phases with MA-Triangular-Prism Bilayers and Elastic Properties, *Angew. Chem., Int. Ed.* **58:** 4576-4580. DOI: 10.1002/ange.201814128

El-Raghy T, Barsoum MW, Zavaliangos A and Kalidindi SR (1999), Processing and mechanical properties of Ti_3SiC_2: II, effect of grain size and deformation temperature, *J. Am. Ceram. Soc.* **82**: 2855-2860. DOI: 10.1111/j.1151-2916.1999.tb02167.x

Fischer TH and Almlof J (1992), General methods for geometry and wave function optimization, *J. Phys. Chem*. **96**: 9768. DOI: 10.1021/j100203a036

Griseri M, Tunca B, Huang Dahlqvist S, Rosén J, Lu J, Persson POA, Popescu L, Vleugels J and Lambrinou K (2020), Ta-based 413 and 211 MAX phase solid solutions with Hf and Nb, *J. Eur. Ceram. Soc.* **40:** 1829-1838. DOI: 10.10 16/j.jeu rcera msoc. 2019 .12.052

He H, Jin S, Fan G, Wang L, Hu Q and Zhou A (2018), Synthesis mechanisms and thermal stability of ternary carbide Mo_2Ga_2C, *Ceram. Int*. **44:** 22289-22296. DOI: 10.1016/j.ceramint.2018.08.353

Hadi MA (2016), New ternary nanolaminated carbide Mo_2Ga_2C: A first-principles comparison with the MAX phase counterpart Mo_2GaC, *Comp. Mater. Sci.* **117**: 422-427. DOI: 10.1016/j.commatsci.2016.02.018

Hadi MA, Kelaidis N, Naqib SH, Chroneos A and Islam AKMA (2009), Mechanical behaviors, lattice thermal conductivity and vibrational properties of a new MAX phase Lu_2SnC, *J. of Phys. And Chem. Of solids* **129**: 162. DOI: 10.1016/j.jpcs.2019.01.009

Hill R (1952), The Elastic Behaviour of a Crystalline Aggregate, *Proc. Phys. Soc. Lond.* **65**: 350. DOI: 10.1088/0370-1298/65/5/307

Jovic VD, Jovic BM, Gupta S, El-Raghy T and Barsoum MW (2006), Corrosion behavior of select MAX phases in NaOH, HCl and H_2SO_4, *Corr. Sci.* **48**: 4274-4282. DOI: 10.1016/j.corsci.2006.04.005

Kohn W and Sham L (1965), Self-Consistent Equations Including Exchange and Correlation Effects, *Physical Review* **140**(4A): 1133-1138. DOI: 10.1103/PhysRev.140.A1133

Karkour S, Bouhemadou A, Allali D, Haddadi K, Bin-Omran S, Khenata R, Al-Douri Y, Ferhat Hamida A, Hadi A and Abd El-Rehim AF (2022), Structural, elastic, electronic and optical properties of the newly synthesized selenides Tl2Cd X Se4 (X= Ge, Sn), *The European Physical Journal B* **95**(3): 38. DOI: 10.1140/epjb/s10051-022-00288-y

Ledbetter HM (1977), Elastic Properties of Zinc: A Compilation and Review, *J. Phys. Chem*. **6**(4): 1181-1201. DOI: 10.1063/1.555564

Lapauw T, Tunca B, Potashnikov D, Pesach A, Ozeri O, Vleugels J and Lambrinou K (2018), The double solid solution $(Zr,Nb)_2(Al, Sn)C$ MAX phase: a steric stability approach, *Sci. Rep.* **8**: 12801. DOI: 10.103 8/s4 1598-018-31271-2

Miao N, Wang J, Gong Y, Wu J, Niu H, Wang S, Li K, Oganov AR, Tada T and Hosono H (2020), Computa-

tional Prediction of Boron-Based MAX Phases and MXene Derivatives, *Chem. Mater.* **32**: 6947-6957. DOI: 10.1021/acs.chemmater.0c02139

Monkhorst HJ and Pack JD (1976), Special points for Brillouin-zone integrations, Phys. Rev. B: Solid State, 13: 5188. DOI: 10.1103/PhysRevB.13.5188

Naguib M, Kurtoglu M, Presser V, Lu J, Niu J, Heon M, Hultman L, Gogotsi Y and Barsoum MW (2011), Two-Dimensional Nanocrystals: Two-Dimensional Nanocrystals Produced by Exfoliation of Ti_3AlC_2., *Adv. Mater.* **23**: 4248-4253. DOI: 10.1002/adma.201190147

Nielsen OH and Martin RM (1983), First-principles calculation of stress, Phys. Rev. Lett. 50: 697. DOI: 10.1103/-PhysRevLett.50.697

Perdew JP, Burke K and Ernzerhof M (1996), Generalized Gradient Approximation Made Simple, *Phys. Rev. Lett*. **77**: 3865-3868. DOI: 10.1103/PhysRevLett.77.3865

Pugh SF (1954), XCII. Relations between the elastic moduli and the plastic properties of polycrystalline pure metals, The London, Edinburgh and Dublin Philos, Mag. *J. Sci.* 45((367): 823–843. DOI: 10.1080/14786440808520496

Qureshi MW, Ma X, Tang G and Paudel R (2021), Ab initio predictions of structure and physical properties of the Zr_2 GaC and Hf_2 GaC MAX phases under pressure, *Sci. Rep.* **11:** 3260. DOI: 10.1038/s41598-021-82402-1

Rackl T, Eisenburger L, Niklaus R and Johrendt D (2019), Syntheses and physical properties of the MAX phase boride Nb2SB and the solid solutions $Nb_2SB_xC_{1-x}$(x-=0-1), *Phys. Rev. Mater.* **3**: 054001. DOI: 10.1103/-PhysRevMaterials.3.054001

Rackl T and Johrendt D (2020), The MAX phase borides Zr_2SB and Hf_2SB, *Solid State Sci*, **106**: 106316. DOI: 10.1016/j.solidstatesciences.2020.106316

Roknuzzaman M, Hadi MA, Ali MA, Hossain MM, Jahan N, Uddin MM, Alarco JA and Ostrikov K (2017), First hafnium-based MAX phase in the 312 family, Hf_3AlC_2: A first-principles study, *J.Alloys Compd.* **727:** 616-626. DOI: 10.1016/j.jallcom.2017.08.151

Ranganathan SI and Ostoja-Starzewski M (2008), Universal Elastic Anisotropy Index, *Phys. Rev. Lett.*, **101**(5): 055504. DOI: 10.1103/PhysRevLett.101.055504

Sun ZM, Hashimoto H, Zhang ZF, Yang SL and Tada S (2006), Synthesis and Characterization of a Metallic Ceramic Material-Ti_3SiC_2, *Mater. Trans*. **47**: 170 -174. DOI: 10.2320/matertrans.47.170

Sundberg M, Malmqvist G, Magnusson A and El-Raghy T (2004), Alumina forming high temperature silicides and carbides, Ceram. Int. **30:** 1899-1904. DOI: 10.1016/j.ceramint.2003.12.046

Surucu G (2018), Investigation of structural, electronic, anisotropic elastic, and lattice dynamical properties of MAX phases borides: An *Ab-initio* study on hypothetical M_2AB (M = Ti, Zr, Hf; A = Al, Ga, In) compounds, *Mater. Chem. Phys.* **203:** 106-117. DOI: 10.1016/j.-matchemphys.2017.09.050

Sokol M, Natu V, Kota S and Barsoum MW (2019), On the Chemical Diversity of the MAX Phases, *Trends Chem.* **1:** 210-223. DOI: 10.1016/j.trechm.2019.02.016

Sin'ko GV and Smirnov NA (2002), Relative stability and elastic properties of hcp, bcc, and fcc beryllium under pressure, Sin'ko GV and Smirnov NA (2005), *Phys. Rev.* B **71:** 214108. DOI: 10.1103/PhysRevB.71.214108

Tunca B, Lapauw T, Delville R, Neuville DR, Hennet L, Thiaudière Ouisse D, Hadermann J, Vleugels J and Lambrinou K (2019), Synthesis and Characterization of Double Solid Solution $(Zr,Ti)_2(Al,Sn)C$ MAX Phase Ceramics, *Inorg. Chem*. **58**: 6669-6683. DOI: 10.1021/acs.inorgchem.9b00065

Tao Q, Lu J, Dahlqvist M, Mockute A, Calder S, Petruhins A, Meshkian R, Rivin O, Potashnikov D, Caspi EN, Shaked H, Hoser A, Opagiste C, Galera RM, Salikhov R, Wiedwald U, Ritter C, Wildes AR, Johansson B, Hultman L, Farle M, Barsoum MW and Rosen J (2019), Atomically Layered and Ordered Rare-Earth i -MAX Phases: A New Class of Magnetic Quaternary Compounds, *Chem. Mater.* **31**: 2476-2485. DOI: 10.1021/acs.chemmater.8b05298

Vanderbilt D (1990), Soft self-consistent pseudopotentials in a generalized eigenvalue formalism, *Phys. Rev. B: Condens*. **41**: 7892. DOI: 10.1103/PhysRevB.41.7892

Voigt W (1928), Lehrbuch der Kristallphysik, Taubner, Leipzig. DOI: 10.1002/zamm.19290090104

Zhang Q, Zhou Y, San X, Li W, Bao Y, Feng Q, Grasso S, Hu C (2022), Zr_2SeB and Hf_2SeB: Two new MAB phase compounds with the Cr_2AlC-type MAX phase (211 phase) crystal structures, *Journal of Advanced Ceramics* **11**(11): 1764-1776. DOI: 10.1007/ s40145- 022-0646-7